Available online at www.sciencedirect.com
SCIENCE DIRECT
Acta Materialia 54 (2006) 1323–1334
Acta MATERIALIA
www.actamat-journals.com

Crystallographic relations between face- and body-centred cubic crystals formed under near-equilibrium conditions: Observations from the Gibeon meteorite

Youliang He [a,*], Stéphane Godet [b], Pascal J. Jacques [b], John J. Jonas [a]

[a] Department of Materials Engineering, McGill University, 3610 University Street, Montreal, Que., Canada H3A 2B2
[b] Département des Sciences des Matériaux et des Procédés, IMAP, Université catholique de Louvain, Place Sainte Barbe 2, B-1348 Louvain-la-Neuve, Belgium

Received 22 June 2005; received in revised form 21 October 2005; accepted 2 November 2005
Available online 6 January 2006

Abstract

The orientations of the kamacite lamellae formed from a single prior-taenite grain were measured by analysing the electron backscatter diffraction patterns obtained using scanning electron microscopy. These are shown to be close to the Kurdjumov–Sachs and Nishiyama–Wassermann relations and their intermediate, i.e., the Greninger–Troiano relation. The orientations of the α grains in the plessite regions were also measured and these were found to be continuously distributed around the Bain circles formed by the variants of the common correspondence relationships, including the Pitsch one in this case. The local misorientations between individual face- and body-centred cubic crystals along their common interfaces were measured. These can be characterized by the orientation relationships mentioned above as long as a certain amount of tolerance is allowed. Orientation variations within individual kamacite lamellae were also analysed. The crystallographic data support the view that somewhat different mechanisms are involved in the formation of Widmanstätten structures and of the plessite in meteorites.

Keywords: Phase transformation; Misorientation; Meteorites; EBSD

1. Introduction

Meteorites have long been of interest to mineralogists and geologists because of their importance in increasing our understanding of the origin and history of asteroidal bodies. Many investigations, e.g., Refs. [1–6], have been carried out to characterize the macro- and microstructures of iron meteorites and to comprehend the formation of the Widmanstätten patterns found within them. Due to certain similarities between metallic meteorites and engineering alloys, meteorites are also of interest to metallurgists. Historically, even the invention of metallography was motivated by the study of meteorites [7] and the construction of the first iron–nickel phase diagram was based on information from iron meteorites [8–11]. The cooling rates deduced from the analysis of Widmanstätten structures have now become useful tools for determining the thermal history of asteroidal bodies [8,12–14].

Although there is still some dispute regarding the mechanism of formation of the Widmanstätten structures, e.g., Refs. [3,8,15,16], these are now generally believed to have formed as the iron meteorites cooled from an initially homogeneous γ-iron phase into the $\alpha + \gamma$ phase field at cooling rates of one to a few hundred degrees per million years [12,13,16–19]. By contrast, for the formation of plessite, a martensitic transformation and decomposition process is generally assumed to have occurred [15,16,20,21]. In order to throw light on these mechanisms, the orientation relationships between the α and γ phases produced during cooling can be examined. Thus, considerable work

* Corresponding author. Tel.: +1 514 398 4755; fax: +1 514 389 4492.
E-mail address: youliang.he@elf.mcgill.ca (Y. He).

1359-6454/$30.00
doi:10.1016/j.actamat.2005.11.008

has been focused on the crystallographic features of the Widmanstätten structures and the plessite found in meteorites.

An early study by Young [22] on the Carlton meteorite carried out using X-ray diffraction resulted in the proposal of an orientation relationship that is actually identical to the later well-known Kurdjumov–Sachs (K–S) relation. In their study of the Bethany meteorite using transmission electron microscopy, Hasan and Axon [23] showed that the orientation relationship of the primary kamacite with respect to the taenite is close to the Nishiyama–Wassermann (N–W) relation, whereas for the plessite kamacite it is close to the K–S relation.

More recently, neutron diffraction methods have been employed to measure the pole figures of both taenite and kamacite crystals in the Gibeon meteorite [24] and the orientations between the kamacite lamellae and the taenite were observed to be close to the N–W relationship. Bunge et al. [25] measured the orientation distributions of the Widmanstätten plates in a sample of the Gibeon meteorite using high-energy synchrotron radiation. Their measurements revealed a continuous range of orientations stretching out from both sides of the N–W orientation to the two adjacent K–S orientations. Electron backscatter diffraction (EBSD) measurements on the Gibeon and other meteorites [26–28] have also produced similar results.

However, none of these studies has provided information about the orientation distribution of individual kamacite lamellae within specimens and about how these orientations vary within a particular α grain. These aspects are the subjects of the present study. Moreover, local orientation relations along the γ/α boundaries were also measured and compared with the common orientation relationships. These are intended to assist in interpreting the mechanisms proposed to explain the formation of Widmanstätten patterns and plessite structures in meteorites. Here, the orientations of both the body-centred cubic (bcc) and face-centred cubic (fcc) phases were measured simultaneously by means of EBSD techniques and the orientation relationships observed are represented in pole figure form as well as in Rodrigues–Frank (R–F) space.

2. Method

The material investigated was a piece of an iron meteorite collected from the Gibeon shower. It consists principally of iron and nickel, together with some trace elements. The main chemical composition is (wt.%) Ni 7.93, Co 0.41, P 0.04 and balance Fe [3]. The Gibeon is classified as falling into the fine octahedrite category (Group IVA). The piece examined here was a slice weighing about 103 g and measuring approximately 60 mm × 60 mm × 5 mm; it was cut from a larger sample.

Ordinary metallographic methods, i.e., optical microscopy, were employed to reveal first the Widmanstätten pattern and then the major phases and microconstituents of the meteorite. Automated EBSD systems equipped with TSL and HKL Channel 5 software in field emission gun scanning electron microscopes were used as the main tools to measure the orientations of the fcc and bcc phases. A small specimen (25 mm × 15 mm) was sectioned from the available piece and a smooth surface was produced by grinding and polishing. Nital (2%) was employed for revealing the Widmanstätten pattern. For microstructural characterization, an aqueous solution containing 10% sodium thiosulphate ($Na_2S_2O_3$) and 3% potassium metabisulphite ($K_2S_2O_5$) was also utilized to decorate various phases in different colours. For the EBSD measurements, after the usual grinding and polishing procedure, the specimen was finally polished using a 0.05 μm colloidal silica suspension in a vibratory finishing machine or by hand on a conventional polishing cloth; the duration of such final polishing was approximately one hour.

The major phases of the Gibeon meteorite are kamacite (ferritic iron with up to 7.5% nickel), taenite (fcc austenite with more than 25% nickel) and plessite, a mixture of both phases. Depending on the nickel content, the lattice parameters of the taenite and kamacite vary slightly. The measured lattice parameters for taenite and pure fcc iron–nickel alloys are in the range of about 0.351–0.360 nm and those for kamacite and bcc iron–nickel fall between 0.286 and 0.289 nm [22,29,30].

EBSD maps were collected using typical settings for steels, e.g., 20 kV, 70° tilt. The measured orientations were represented in the format of Euler angles with respect to the sample reference frame. For metal processing, this is usually directly related to the reference directions of materials processing. However, in the case of meteorites, there are no meaningful reference directions. The orientations of both the fcc and bcc phases were measured simultaneously in each EBSD scan. Other phases (e.g., martensite), inclusions, small particles and grain boundaries could not be identified and remained unresolved on the EBSD maps. The angular accuracy of the EBSD system is about 1° using the operational parameters for meteorites and steels. The orientations measured within a ferrite grain transformed from deformed austenite in a transformation-induced plasticity steel indicate a spread of less than 1° [31].

3. Results

3.1. The Widmanstätten pattern and microstructures

An example of the Widmanstätten pattern revealed by optical microscopy is illustrated in Fig. 1(a). It is evident that the kamacite lamellae cross each other at various angles and enclose areas of grey or dark plessite of different sizes between them. The detailed microstructures can be seen more clearly in Fig. 1(b) and (c); here tint etching was carried out using the solution mentioned above. The three major phases, namely kamacite, taenite and plessite, can be readily distinguished. The kamacite lamellae, which are about 0.3 ± 0.05 mm in thickness, are in colour and are sheathed by thin white films of taenite. Within the kamacite

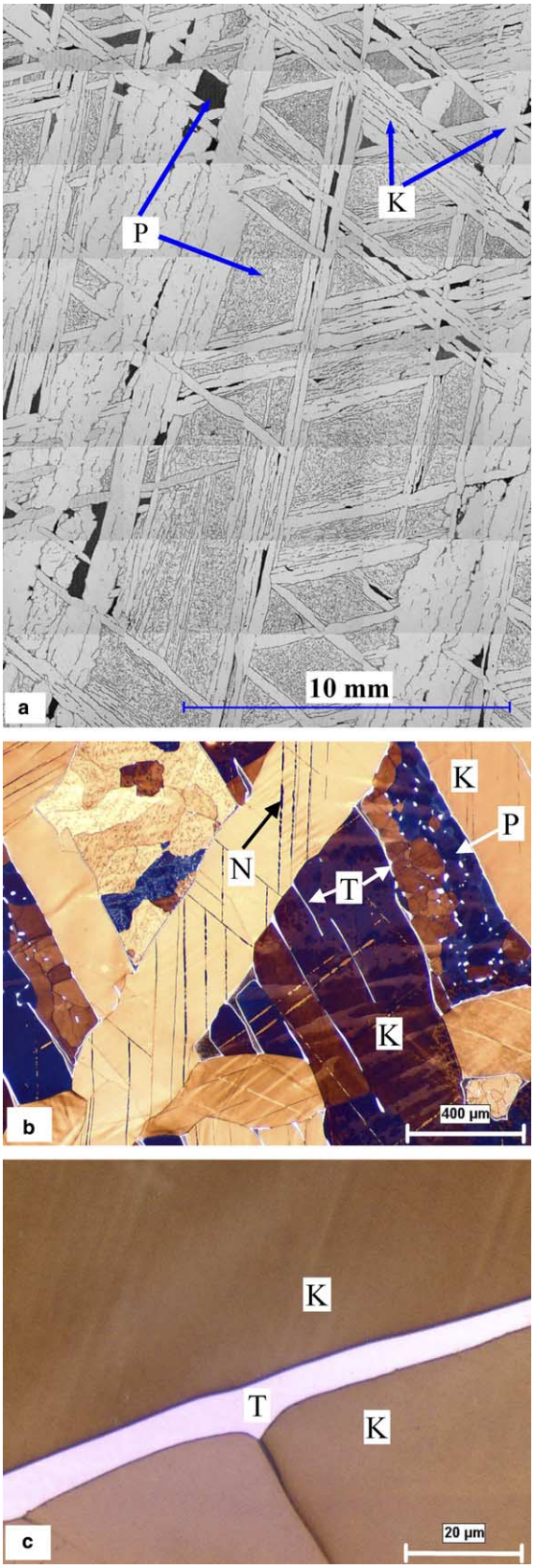

Fig. 1. Optical micrographs of the Gibeon meteorite: (a) Widmanstätten structure revealed by etching with 2.0% nital; (b) a region containing the four common microstructural features: kamacite (K), taenite (T), plessite (P) and Neumann bands (N); (c) enlarged view of a taenite film between kamacite lamellae.

lamellae, numerous Neumann bands (mechanical twins) can be seen. These are believed to have formed as a result of extraterrestrial collisions, not by impact with the earth [3,6]. An example of Neumann bands crossing a kamacite lamella is displayed in Fig. 1(b). An enlarged view of the taenite film between two kamacite lamellae is shown in Fig. 1(c), where the thickness of the taenite film is about 10 μm.

Plessite fields are usually outlined by a number of faceted sides and display different microstructures. As illustrated in Fig. 2, three different types of plessite region can be distinguished. The first type (1) is net plessite (Fig. 2(b)), which consists mainly of equiaxed kamacite grains with many boundaries and sub-boundaries. Taenite appears as small islands (usually 1–10 μm in size) at grain boundaries or within the kamacite grains. The second type (2) is cellular plessite (Fig. 2(c)), which is composed of kamacite aggregates (cells) framed by taenite. Within each kamacite aggregate, there are numerous tiny taenite particles. The third type (3) is finger plessite, which appears black and unresolvable at low microscope magnification. However, under higher magnification, it is apparent that this structure contains elongated α crystals that follow the Widmanstätten directions (bright laths in Fig. 2(d)).

3.2. Orientation relations between the kamacite lamellae and the retained taenite

The prior-taenite grain size of the Gibeon meteorite is very large, typically 10–50 cm [3], with the kamacite lamellae being about 0.3 mm wide. In the piece of the Gibeon meteorite investigated, no prior-taenite grain boundary was observed. Thus all the kamacite lamellae originated from the same prior-taenite grain. Since the widths of the kamacite lamellae were of the order of hundreds of micrometers, the step size of the EBSD scans was selected to be as large as 50 μm. In this way, more kamacite lamellae could be covered in each scan. A total of 8 orientation maps was obtained, which covered an area of about 170 mm^2. The measured orientation maps are illustrated in Fig. 3 in inverse pole figure form.

Once the orientations of both the kamacite and taenite phases were measured, it was possible to investigate the orientation relationships directly by plotting them in an appropriate orientation space. In order to reduce the level of uncertainty caused by the large step size, only orientations with confidence index values greater than or equal to 0.4 were used. In this case, 57 taenite (austenite) points were collected and their orientations are shown in Fig. 4(a). It is evident that the taenite fragments share an almost identical orientation, with an average spread of 4°. Their mean orientation is ($\varphi_1 = 100.7°$, $\Phi = 51.4°$, $\varphi_2 = 30.9°$), as described by the three Euler angles. The orientations of the kamacite lamellae are illustrated in Fig. 4(b), where it is evident that these cluster around the three reflections of the taenite orientation.

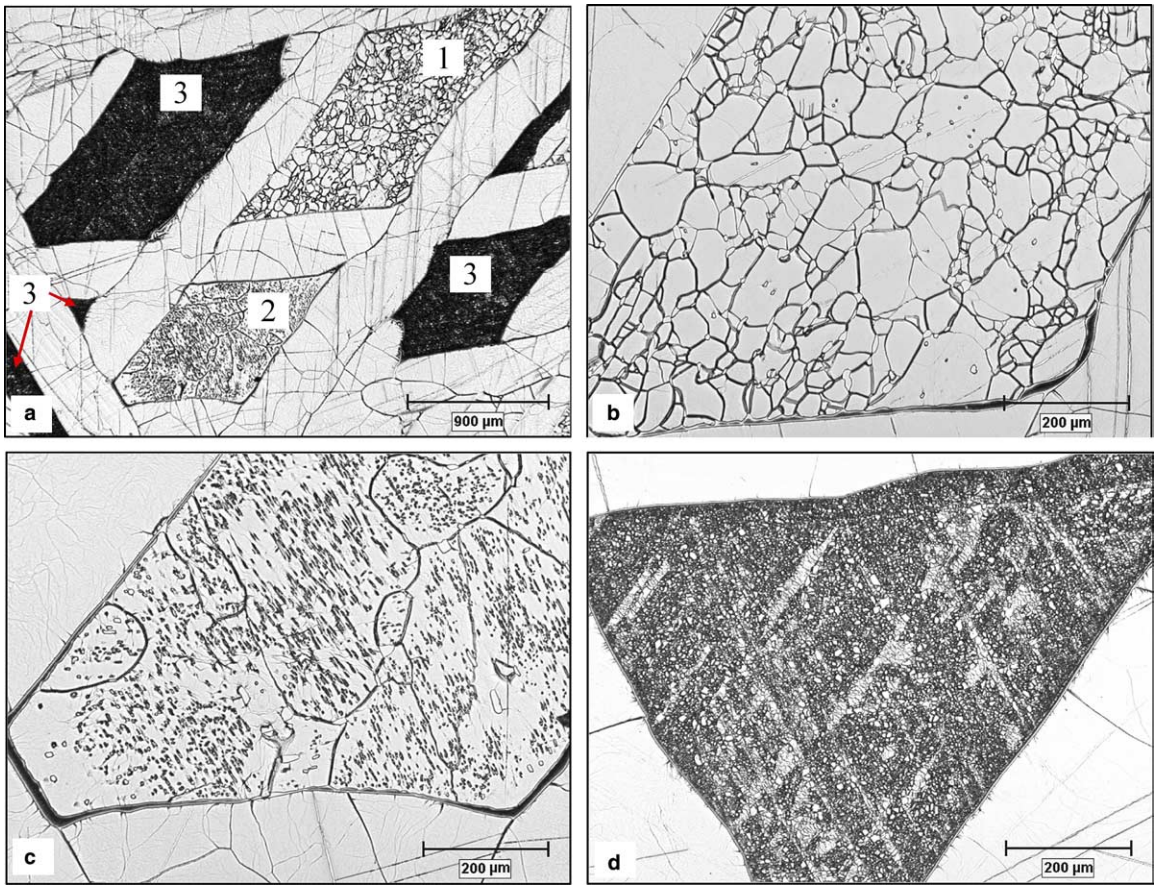

Fig. 2. Optical micrographs of various plessite morphologies: (a) region showing three types of plessite field; (b) net plessite; (c) cellular plessite; (d) finger plessite (etched with 2% nital).

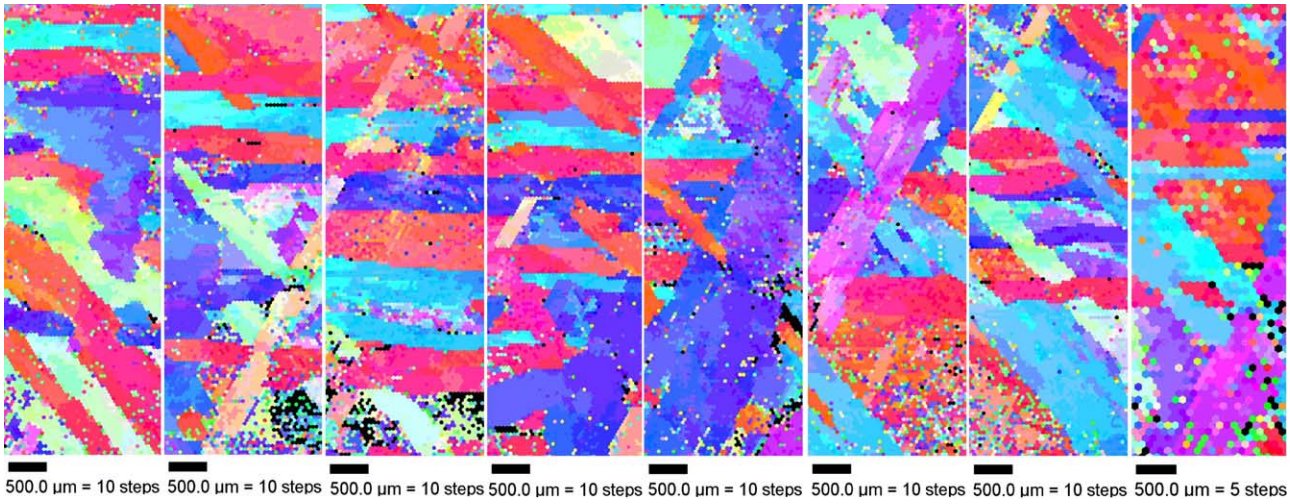

Fig. 3. Inverse pole figure maps of the 8 scans. The total scanned area is about 170 mm^2.

Fig. 4(c) illustrates the kamacite orientations plotted on a pole figure referred to the γ coordinate system. Also displayed are the Bain, K–S, N–W and Pitsch variants predicted from the mean orientation of the taenite. It is apparent that most of the kamacite orientations cluster around the N–W positions and extend continuously towards the neighbouring K–S variants. It has already been demonstrated elsewhere [32–34] that a Greninger–Troiano (G–T) [35] variant is present approximately midway between each pair of adjacent N–W and K–S variants. Thus it is clear that the orientation relationship between the kamacite lamellae and the taenite is not unique, but

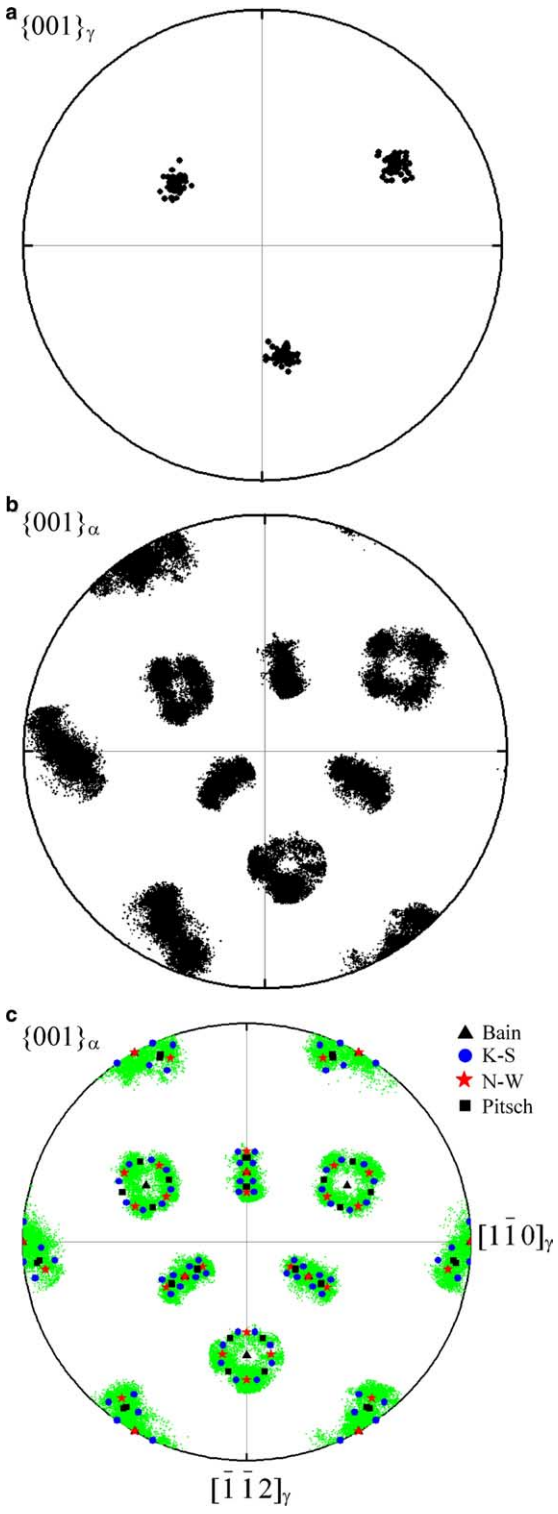

Fig. 4. Orientations of the taenite and kamacite phases: {001} pole figures of (a) the taenite and (b) the kamacite (here the orientations are referred to the data acquisition coordinate system). (c) Kamacite orientations plotted on a pole figure referred to the mean taenite coordinate system, together with the Bain, K–S, N–W and Pitsch variants predicted from the mean orientation of the taenite.

covers a continuous distribution from the N–W, through the intermediate G–T, to the K–S. Although some orientations are found to be located near the Pitsch [36] reflections, their intensities are relatively small. The Bain variants, which are located at the centres of the circles, are not observed. It is also evident that almost all the K–S and N–W variants are present, which indicates that no variant selection occurred.

It is of interest that, even when the cooling rate is very high, as in welding simulations, an absence of variant selection has been reported [37,38]. Thus, cooling rate does not seem to influence the amount of variant selection when the transformation is intragranular (leading to the formation of bainite or acicular ferrite in the case of plate steels).

These relationships can be seen more clearly in R–F space, as shown in Fig. 5, where the measured kamacite orientations are plotted by taking one of the Bain variants as the reference frame. These are compared against the predictions obtained from the six common correspondence relationships, namely the Bain, K–S, N–W, G–T, Pitsch and G–T′. It should be noted that the G–T′ (inverse G–T) relation is an extension of the G–T relation and is located between the K–S and Pitsch orientations. A detailed description of this new relation can be found in Refs. [32,33]. From Fig. 5, it is again evident that the measured kamacite orientations are spread almost uniformly from the N–W, through the G–T, to the K–S positions, while they are relatively sparse in the neighbourhood of the Pitsch and G–T′ positions.

3.3. Correspondence relationships at the kamacite/taenite boundaries

It has already been established that the relationship between the mean taenite and kamacite lamellae orientations does not exactly follow the K–S, N–W or G–T relations, but that considerable scatter around all these reflections is observed. Since the taenite orientations have an average

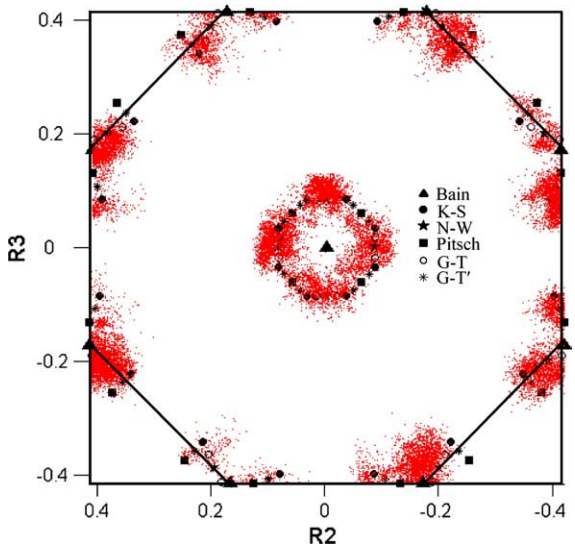

Fig. 5. The kamacite orientations plotted using one of the Bain variants as the reference frame and projected onto the base of the "Bain variant" R–F cube.

deviation of about 4° and all the kamacite orientations are displayed together, it is not clear how the kamacite is related crystallographically to the taenite at specific taenite/kamacite interphase boundaries. It is thus necessary to examine the orientations of the kamacite grains immediately next to a specific taenite crystallite. This can be done by calculating the *misorientations* between the taenite and kamacite crystals along their mutual interfaces and comparing these to the common correspondence relationships.

Since the retained taenite usually consists of films <10 μm in thickness or of blebs less than a few micrometers in diameter, it is essential to employ a small enough step size to measure correctly the orientations of the taenite phase. For this purpose, a step size of 0.8 μm was utilized. Each of the orientation and phase maps obtained in this way is illustrated in Fig. 6. It is clear that most of the taenite is retained in the form of rims framing the plessite regions, e.g., a net plessite field is detected in the centre. The taenite layers abut both the kamacite lamellae and the plessite fields. Blebs of retained taenite are also found within the plessite region.

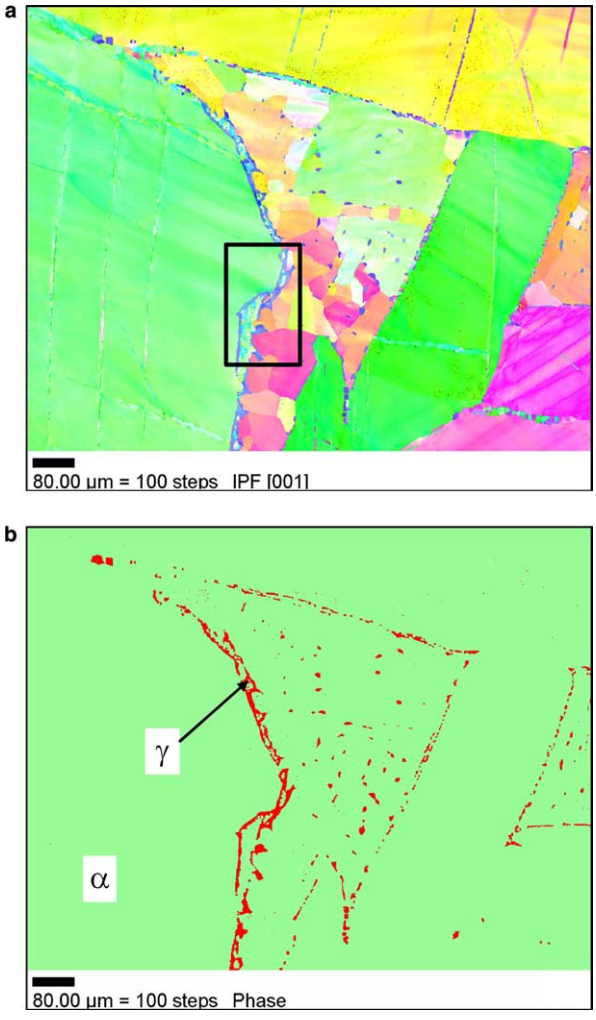

Fig. 6. EBSD maps obtained using a step size of 0.8 μm: (a) orientation map; (b) phase map.

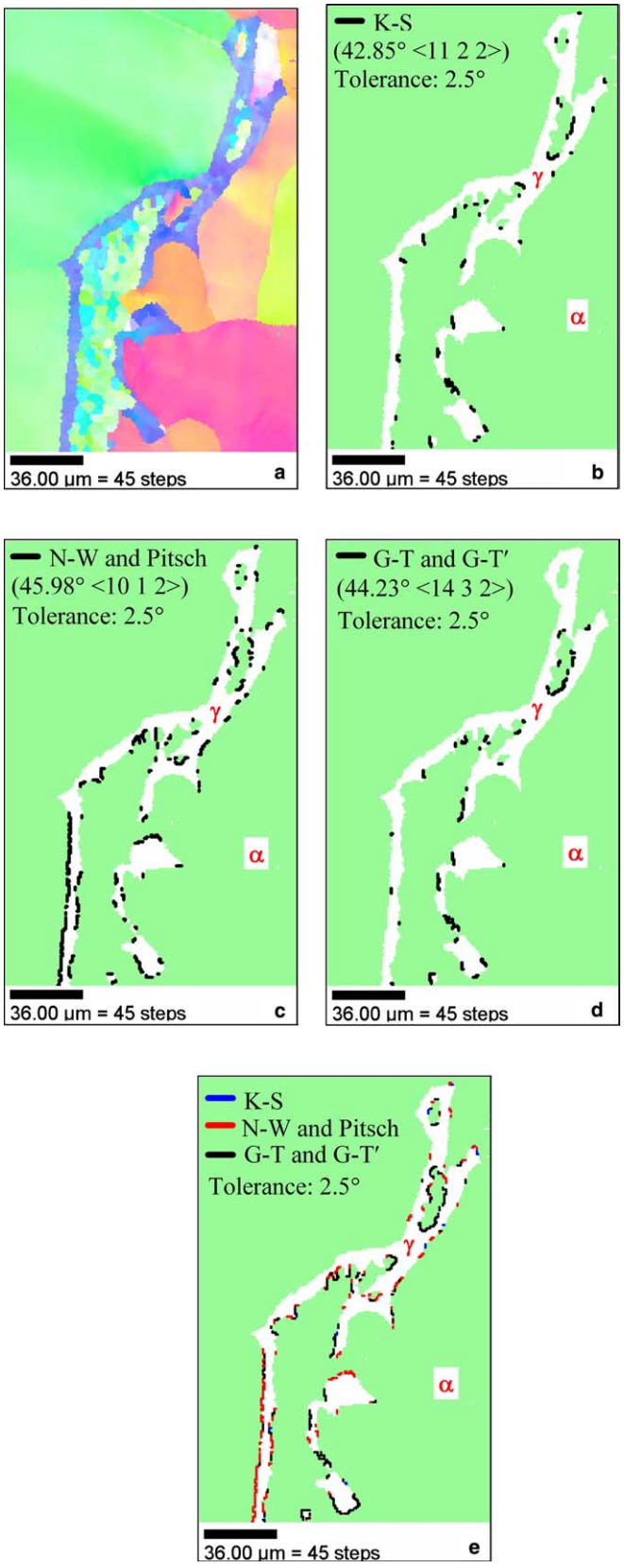

Fig. 7. Misorientations between an fcc crystal and several bcc crystals along their common interfaces: (a) inverse pole figure map showing the orientations of the two phases; (b) K–S; (c) N–W and Pitsch; (d) G–T and G–T′; (e) all five boundaries shown highlighted. Here a 2.5° tolerance is employed for all the correspondence relations.

In order to inspect the orientation relationships between the γ and α phases along their common interfaces, a portion of these boundaries (identified by the rectangle in Fig. 6(a)) is highlighted in Fig. 7(a). The misorientations between these two phases along the boundaries are compared to the five main orientation relationships (except for the Bain relation) in Fig. 7(b)–(e). It should be mentioned that the misorientations were calculated based on the orientations collected from the fcc and bcc points (pixels) that are immediately next to each other in the orientation map. These were then compared to the predicted orientations according to the common correspondence models. Although orientation differences exist (usually ~2°) at points away from the interface, the orientation gradients were not observed to be functions of distance from the boundary. Such differences are within the angular accuracy of the EBSD system and thus do not affect the orientation relationships discussed above.

These results make it clear that each of the five relations is obeyed along different portions of the interface as long as a certain amount of tolerance (2.5° in this case) is allowed. It should be noted that a significant proportion of each boundary does not obey any of the relations. This means that the exact orientation relationships prescribed by these models are not followed at all points of the γ/α interface. Indeed, deviations are found from the ideal misorientations in portions of *all* the boundaries. Since the N–W and Pitsch relations involve the same rotation angle and rotation axis components (but permuted in a different order [28]), they could not be distinguished using the EBSD software. Similar remarks apply to the G–T and G–T′ relations [32].

3.4. Orientation variations in the kamacite lamellae

One of the most attractive features of the EBSD technique is that both microstructural and crystallographic information regarding the specimen can be obtained simultaneously. This makes possible the investigation of the crystallographic features of specific microstructures. In the case of the iron meteorite, it is of particular interest to examine the orientation variations within individual kamacite lamellae that usually extend along millimeters or even centimeters.

Examples of the orientation variations within individual α grains are illustrated in Fig. 8. It is apparent from the misorientation profiles (Fig. 8(b) and (c)) that the orientation within a particular kamacite lamella can vary by up to about 10°, with numerous Neumann bands (twins, of 60° misorientation) in one of the profiles. Since the orientation change within a single kamacite lamella approaches the misorientation angle between neighbouring K–S variants (10.53°), it is of interest to compare these variations to the predictions of the various models.

The orientation spread of kamacite lamella 1 in Fig. 8(a) is shown in pole figure form in Fig. 8(d). It is evident from the enlarged view (Fig. 8(e)) of Fig. 8(d) that, within one lamella, the local orientations include the two coplanar K–S variants (i.e., **cI** and **–cII**, which have the same plane parallelism condition [28]), together with the intermediate N–W and G–T variants. In martensite, such low-misorientation variants have been identified by Morito et al. [39] as belonging to a single lath with a well-defined {1 1 1} habit plane. A single twin-related orientation can also be seen (near **–cI**, which is the twin-related variant of **cI**). The orientation profiles collected from other lamellae have similar features.

It can thus be concluded that, within each kamacite lamella, the orientation is not unique, but a spread of up to about 10° can be observed; these typically extend between the reflections of two coplanar K–S variants and thus cover their intermediates. Also apparent are the numerous twins within each lamella.

3.5. Crystallographic features of the plessite regions

It has been pointed out that three types of plessite were found in the sample of the Gibeon meteorite investigated. The microstructural and stereological aspects of the plessite fields in this meteorite have previously been studied by Ryder and Howell [20]. However, their crystallographic features, i.e., the orientation relationship between the taenite and kamacite in this two-phase mixture, have not been studied intensively. Nevertheless, an investigation by Hasan and Axon [23] using transmission electron microscopy indicated that there was a near K–S relationship between the two phases.

Here, a typical finger plessite field was investigated by means of EBSD. In order to reveal the fine structure of the region, an even smaller step size (0.2 μm) was employed to scan the 325 × 224 μm area shown in Fig. 9(a). The EBSD maps obtained are displayed in Fig. 9(b)–(d).

The image quality map of Fig. 9(b) reveals the microstructure of the finger plessite. Starting from the kamacite lamella inward, there appears a layer of taenite, followed by a martensite zone (dark). In the interior, there are mostly lath-like α grains. The morphologies and orientations of these two phases can be seen more clearly in the α and γ orientation maps of Fig. 9(c) and (d), respectively. Examination of the orientations of the lath-like kamacite grains in the interior of Fig. 9(c) indicates that many of these laths share the orientations of the two adjoining kamacite lamellae (coloured purple in this figure). From the orientation map of the retained taenite, it is apparent that, in the interior, most of the taenite is retained in the form of small particles at the kamacite grain boundaries, but the outline of the plessite region is composed of a continuous taenite film. It is also clear that there is a thin, continuous layer of taenite between the martensite zone and the interior.

The orientations of the taenite in the outer rim and in the interior of the plessite region are represented in Fig. 10(a) and (b), respectively. It is apparent that the retained taenite shares an essentially unique orientation (with more scatter in the interior), whether from the outer rim or from the interior.

The orientations of the kamacite in the plessite field are represented in pole figure form in Fig. 10(c). Here, the

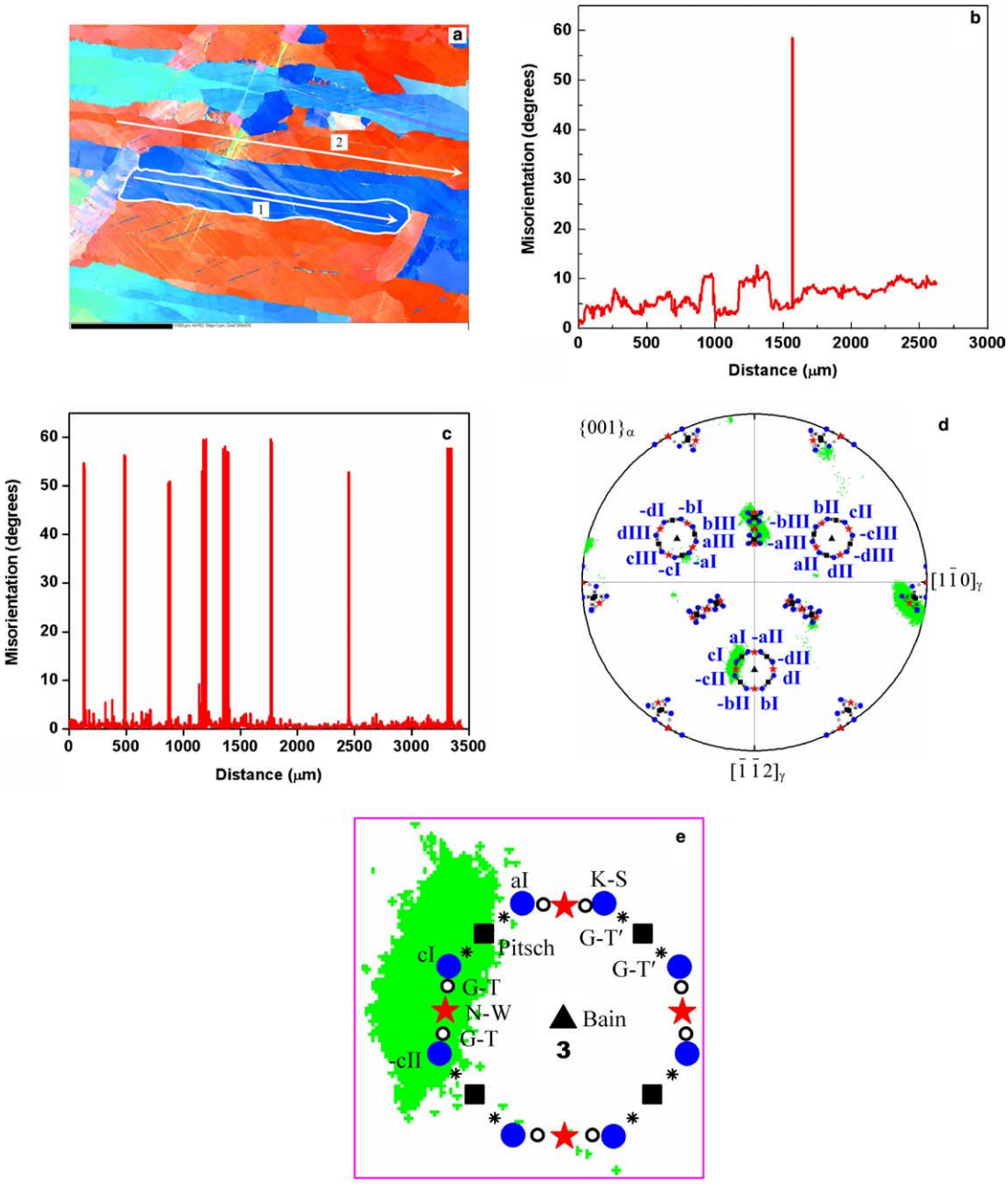

Fig. 8. Orientation variations within kamacite lamellae: (a) inverse pole figure map showing the kamacite orientations; (b) misorientation profile within lamella 1 in (a); (c) misorientation profile within lamella 2 in (a); (d) orientations of lamella 1 displayed in pole figure form; (e) magnified view of one of the Bain clusters in (d) showing the locations of the K–S, N–W, G–T, Pitsch and G–T′ variants.

reference frame is taken as the mean orientation of the taenite retained within the plessite region; the predictions of the Bain, K–S, N–W, Pitsch, G–T and G–T′ relations are also illustrated. It is again evident that the measured kamacite orientations are distributed fairly even around the three Bain circles formed by the variants of the five orientation relationships. In this case, however, the three circles are almost continuously covered by the observations. The reflections that are not observed can be attributed to an incomplete scan of the plessite region shown in Fig. 9(a). Thus the orientation relationship between taenite and kamacite in the plessite region can also be described by the five correspondence relations, although more scatter is observed in this case. It should also be noted that, as in the case of the Widmanstätten structure, no variant selection has occurred in the plessite region.

4. Discussion

4.1. Distribution of the common orientation relationships

Geometrically, the relationships between the phases in the common correspondence models, e.g., the Bain, K–S, N–W and Pitsch, are solely determined by the symmetries

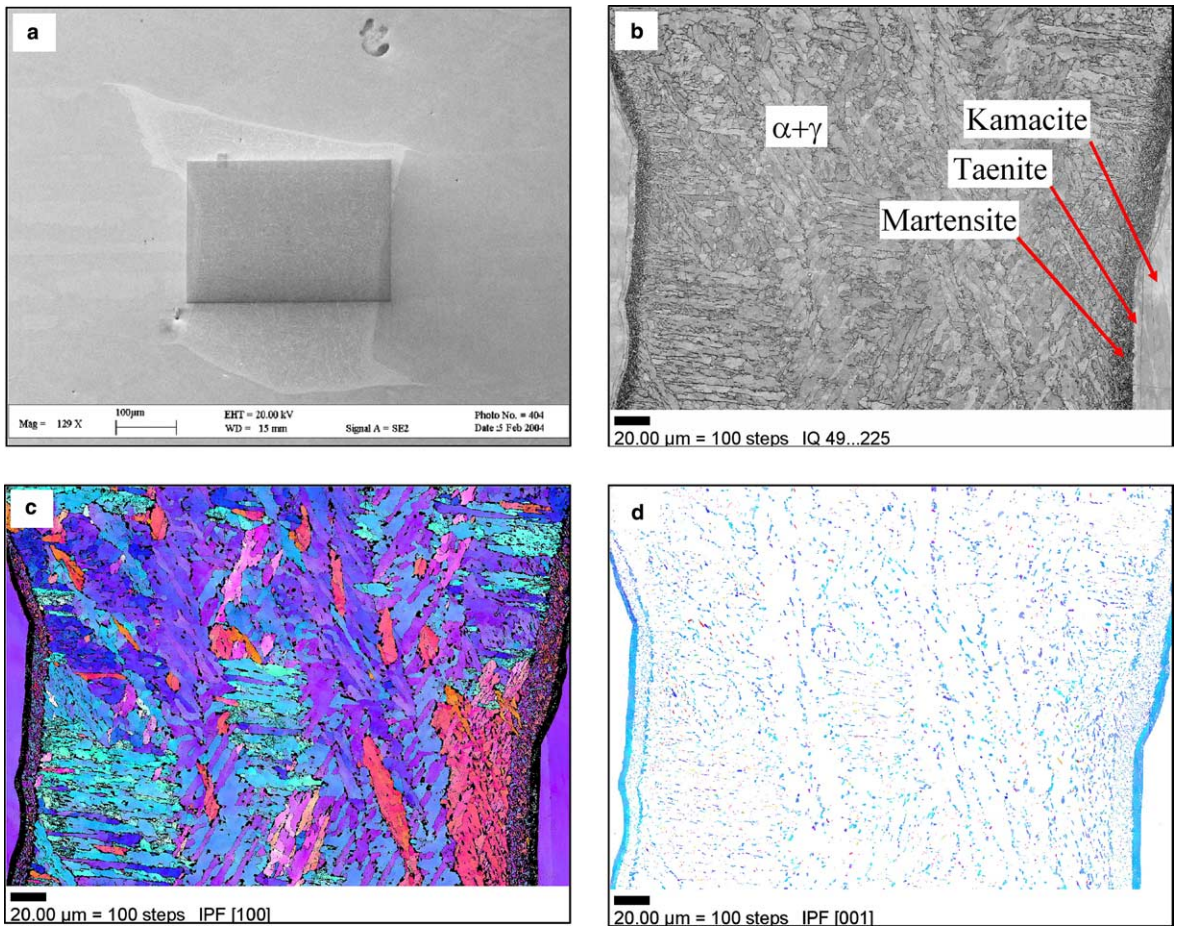

Fig. 9. (a) Scanning electron micrograph showing the scanned plessite region; (b) image quality map; (c) orientations of the α phase; (d) orientations of the γ phase.

of the two lattices involved [34]. For example, the rotation angle of 5.26° (about the normal to the close-packed planes) that brings the N–W into coincidence with the K–S relationship is independent of the relative lattice parameters of the two structures. According to the phenomenological theory of phase transformation, e.g., Refs. [40,41], the orientation relationship is mainly dictated by the Bain strain, which is in turn closely related to the lattice parameters of the two phases. Indeed, in the framework of this theory, the orientation relationship is determined by the rotation required to transform the Bain strain into an invariant line strain. As discussed in more detail by Dahmen [34], for phase transformations involving lattice parameter ratios between 1.21 and 1.36, the rotations associated with various orientation relationships are not expected to differ much. Examination of the taenite and kamacite lattice parameters shows that the $a_{\text{taenite}}/a_{\text{kamacite}}$ ratio falls in the range 1.22 to 1.26, depending on the Ni content of the γ phase. (During cooling, the γ phase is progressively enriched in Ni due to Ni rejection by the increasing volume fraction of the α phase). Thus, the experimental spread in lattice parameter ratios associated with the different Ni contents is not expected to affect the orientation relationship predicted by the phenomenological theory to a measurable degree.

In the present work, the observed orientation relationships between the taenite and kamacite phases were found to extend from one K–S to its coplanar neighbour, passing through the intermediate N–W variant. This is in contradiction to the predictions of the phenomenological theory, which call for K–S at an acceptable parameter ratio of 1.23, but require an out-of-range 1.155 for N–W. As discussed in more detail below, a possible explanation for this discrepancy is that the formation of Widmanstätten ferrite involves a reconstructive mechanism, in which all types of diffusion can take place. Under these conditions, the transformation is governed by the minimization of the interfacial energy, a condition that involves plane-to-plane correspondence. Furthermore, as illustrated in Fig. 7, the orientation relationship varies along the interface of a single kamacite lamella. Such a spread has already been reported by Bunge et al. [25]. In their work, it was proposed that the plane matching condition corresponds to an energetic minimum, whereas the direction parallelism condition does not lead to energy changes over the range (K–S)–(N–W)–(K–S) (i.e., over 10.53°).

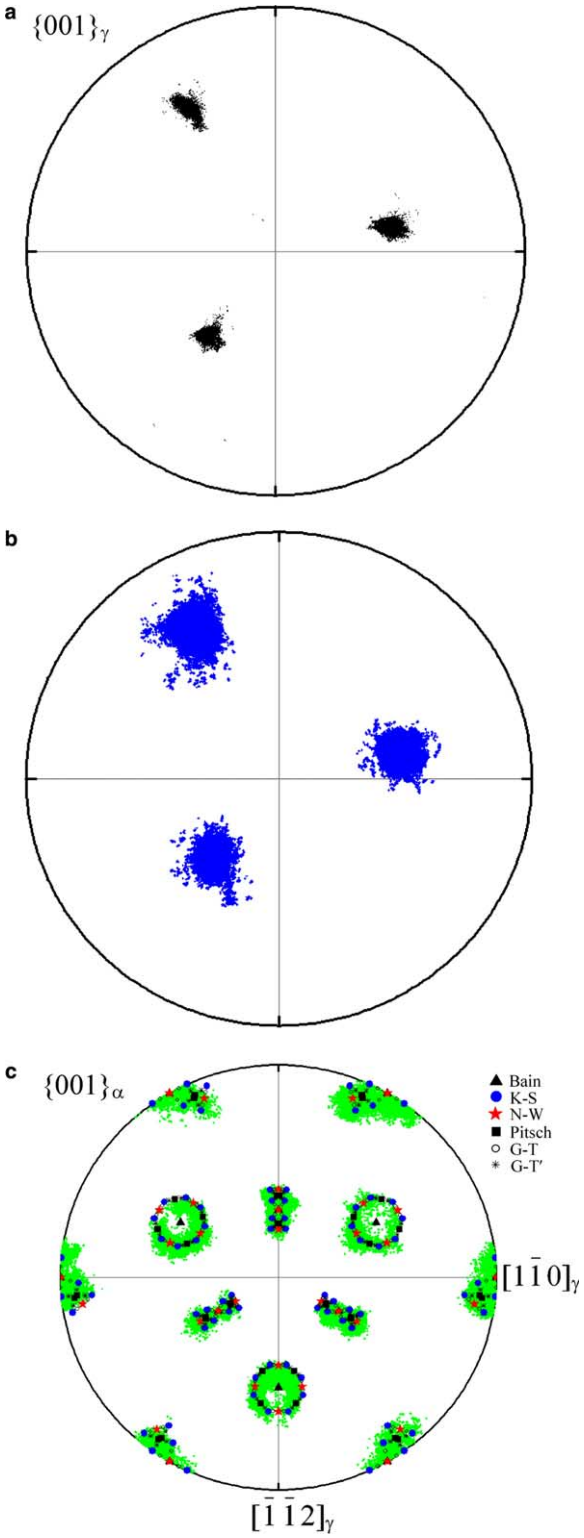

Fig. 10. {001} pole figures of the retained taenite and kamacite in the plessite region: (a) taenite from the outer rim; (b) taenite from the interior of the plessite field; (c) kamacite pole figure referred to the mean orientation in (b), together with the predictions.

In contrast, the orientations detected in the *plessite* regions are evenly distributed around complete Bain circles. The Pitsch relation, originally observed in the precipitation of cementite from austenite [42], was found to be obeyed in addition to those of K–S and N–W. This orientation relationship can be described as $\{0\,0\,1\}_\gamma \| \{1\,0\,1\}_\alpha$ and $\langle 1\,1\,0\rangle_\gamma \| \langle 1\,1\,1\rangle_\alpha$ and is characterized by the parallelism of close-packed *directions*. Evidence for the presence of this orientation relationship in the *macroscopic* measurements of Bunge et al. [25] has also been reported but no explanation was provided. It has been demonstrated by Dahmen [34] as well as by Zhang and Kelly [43] that, during precipitation, the directional matching criterion is more important than the planar one. This is the case for the Pitsch and G–T′ relationships, both of which are associated with the parallelism of close-packed directions. It is therefore of interest to raise the question of whether the crystallographic data gathered in the (taenite + kamacite) region on the one hand and the plessite regions on the other can improve our understanding of the transformation mechanisms that govern the formation of these microstructures.

4.2. Formation mechanisms of the Widmanstätten pattern and plessite

Over the two centuries since the discovery of the Widmanstätten structure in 1808, many mechanisms have been proposed to explain this unique pattern. In the early days, it was believed to form directly by crystallization from a very slowly cooling melt. Nowadays, the controversy is essentially focused on whether it results from the equilibrium transition of γ to $\alpha + \gamma$ [3,15] or is a consequence of a martensitic transformation ($\gamma \rightarrow \alpha_2 + \gamma$) followed by a decomposition process [16].

As described above, the orientation relationships between the taenite and kamacite are close to K–S and N–W together with all the intermediate points. These are consistent with both the $\gamma \rightarrow \alpha + \gamma$ and $\gamma \rightarrow \alpha_2 + \gamma \rightarrow \alpha + \gamma$ mechanisms. The spread of orientation relationships can be taken to support the view that the transformation is diffusionless (i.e., martensitic). Alternatively, the same orientation relationships (K–S and N–W) are observed in steels [44] and in α/β brasses [45], where the transformation is diffusional and Widmanstätten. However, if the Widmanstätten pattern is considered to result from the transformation of martensite, it should be possible to produce this structure in the laboratory. As such observations have never been reported, it seems more reasonable to conclude that this unique pattern forms under diffusional conditions.

The formation of the plessite regions trapped between the Widmanstätten lamellae has also been the subject of many investigations, e.g., Refs. [15,17,18,20,21,46]. In this case, most of the mechanisms proposed involve the formation of martensite and the subsequent decomposition of this metastable phase during cooling or reheating (rewarming). The only points at issue concern whether the formation of plessite is completely associated with the martensite transformation or is only partially related.

It can be seen in Fig. 9(b) that a dark band is present on both sides of the plessite region. Examination of these bands under high magnification reveals that they actually consist of fine grains of α, γ and α_2 (martensite), where the orientations of the α phase obey the K–S and N–W relationships with respect to the γ phase. The bands border the high-Ni taenite layers and have relatively high Ni contents. As can be seen from the Fe–Ni phase diagram presented by Reuter et al. [10], a higher Ni content corresponds to a lower martensite start temperature M_s. Therefore, the martensite reaction in these bands takes place at temperatures where the Ni diffusion rate is low. As a result, the decomposition of α_2 to equilibrium $\alpha + \gamma$ is incomplete and much of the martensite is retained.

In contrast, in the centre of the plessite region, the Ni concentration is much lower than in the region that borders the taenite rim (although is still higher than in the bulk prior to transformation). Because the Ni content is higher than in the initial material, this portion of the taenite starts to precipitate α at a temperature lower than that of Widmanstätten precipitation. Thus the α laths that form in the central portion of the retained taenite are finer than the Widmanstätten lamellae. Some of these α precipitates share the orientations of the Widmanstätten plates, while others form according to the Pitsch and G–T′ relations. Some taenite is also retained, mostly at the boundaries of the α laths.

As described above, the Pitsch and G–T′ orientation relationships (usually observed in precipitates) have been shown to be evenly distributed around the Bain circles in the plessite region. Thus the view that the central plessite regions form by a precipitation process is supported by the crystallographic data obtained in this study.

5. Summary and conclusions

The crystallographic features of the Gibeon meteorite were studied by means of EBSD techniques. The orientations of the bcc phase within the Widmanstätten lamellae and in the plessite regions were measured and compared to the variants predicted by the Bain, K–S, N–W, Pitsch, G–T and G–T′ orientation relationships. The results obtained can be summarized as follows:

1. The Widmanstätten lamellae obey orientation relationships with respect to the original austenite that are close to both the K–S and N–W relations, as well to the intermediate G–T relation. Few reflections are found near the Pitsch and inverse G–T relations. Almost all the expected variants were identified and essentially no variant selection was observed.
2. The observations regarding the transformation of γ into α in the plessite region indicate that both the K–S and N–W relationships are obeyed, together with that called for by the intermediate G–T relation. However, in this case, the Pitsch and inverse G–T reflections are also present with almost equal intensities.
3. The misorientations between individual fcc and bcc crystals along their mutual interfaces indicate that all five relations are obeyed along different portions of the interface (as long as a certain amount of tolerance is allowed). A significant proportion of each boundary does not obey *any* of the relations. This means that the *exact* orientation relationships described by these models are not followed at all points of the γ/α interface.
4. The Bain relationship is never observed in the Widmanstätten structure or in the plessite regions.
5. Orientation deviations of about 10° were found within individual kamacite lamellae; these indicate the presence of a low-misorientation coplanar variant within these lamellae.

Acknowledgements

The authors are grateful to the Natural Sciences and Engineering Research Council of Canada and to the FNRS and FRFC of Belgium (S.G. and P.J.J.) for financial support. S.G. is thankful for a Return Grant from the Belgium Science Policy agency.

References

[1] Chladni E. Feuer Meteore. Vienna; 1819.
[2] Tschermak G. Lehrbuch der Mineralogie; 1894.
[3] Buchwald VF. Handbook of iron meteorites: their history, distribution, composition and structure, vol. I–III. Berkeley, CA: University of California Press; 1975.
[4] Axon HJ. Prog Mater Sci 1967;13:183.
[5] Perry SH. US Natl Museum Bull 1944(184).
[6] Voort GFV. Mater Charact 1992;29:223.
[7] Habashi F. CIM Bull 1995;88:61.
[8] Budka PZ, Viertl JRM, Thamboo SV. Adv Mater Process 1996;7:27.
[9] Osmond F, Cartaud G. Revue de Métallurgie 1904:70.
[10] Reuter KB, Williams DB, Goldstein JI. Metall Trans 1989;20A:719.
[11] Owen EA, Liu YH. J Iron Steel Inst 1949:132.
[12] Goldstein JI, Short JM. Geochim Cosmochim Acta 1967;31:1001.
[13] Goldstein JI, Short JM. Geochim Cosmochim Acta 1967;31:1733.
[14] Wasson JT. Meteorites: their record of early solar system history. New York (NY): WH Freeman; 1985.
[15] Massalski TB, Park FR, Vassamillet LF. Geochim Cosmochim Acta 1966;30:649.
[16] Yang J, Goldstein JI. Meteorit Planet Sci 2005;40:239.
[17] Wood JA. Icarus 1964;3:429.
[18] Short JM, Andersen CA. J Geophys Res 1965;70:3745.
[19] Goldstein JI, Ogilvie RE. Geochim Cosmochim Acta 1965;29:893.
[20] Ryder JM, Howell PR. Microstruct Sci 1998;26:467.
[21] Goldstein JI, Michael JR. Meteorit Planet Sci 2006 (in press).
[22] Young J. Proc R Soc London Ser A 1926;112:630.
[23] Hasan F, Axon AJ. J Mater Sci 1985;20:590.
[24] Höfler S, Will G, Hamm HM. Earth Planet Sci Lett 1988;90:1.
[25] Bunge HJ, Weiss W, Klein H, Wcislak L, Garbe U, Schneider JR. J Appl Cryst 2003;36:137.
[26] Nolze G. Z Metallkd 2004;95:744.
[27] Nolze G, Geist V. Cryst Res Technol 2004;39:343.
[28] He Y, Godet S, Jonas JJ. Acta Mater 2005;53:1179.
[29] Owen EA, Yates EL, Sully AH. Proc Phys Soc 1937;49:315.
[30] McKeehan LW. Phys Rev 1923;21:402.

[31] He Y, Godet S, Jacques PJ, Jonas JJ. Mater Sci Forum 2005;495–497:1201.
[32] Jonas JJ, He Y, Godet S. Mater Sci Forum 2005;495–497:1177.
[33] He Y, Godet S, Jonas JJ. J Appl Cryst 2006 (in press).
[34] Dahmen U. Acta Mater 1982;30:63.
[35] Greninger AB, Troiano AR. Metal Trans 1949;185:590.
[36] Pitsch W. Acta Metall 1962;10:897.
[37] Anelli E, Matera S, Harrison P, Gutiérrez I, Díaz Fuentes M, Porter D, et al. European Commission technical report. EUR 20125 EN; 2002. p. 146.
[38] Lambert-Perlade A, Gourgues AF, Pineau A. Acta Mater 2004;52:2337.
[39] Morito S, Tanaka H, Konishi R, Furuhara T, Maki T. Acta Mater 2003;51:1789.
[40] Wechsler MS, Lieberman DS, Read TA. Trans AIME 1953;197:1503.
[41] Bowles JS, Mackenzie JK. Acta Metall 1954;2:224.
[42] Pitsch W. ArchEisenhüttenwes 1967;38:853.
[43] Zhang MX, Kelly PM. Acta Mater 1998;46:4617.
[44] Bhadeshia HKDH. Bainite in steels. London: IOM Communications; 2001.
[45] Stanford N, Bate PS. Acta Mater 2005;53:859.
[46] Zhang J, Williams DB, Goldstein JI. Geochim Cosmochim Acta 1993;57:3725.